Anisotropic coarsening: One-dimensional decay of Ag islands on Ag(110)

Yong Han,[1] Selena M. Russell,[2,*] Anthony R. Layson,[2,†] Holly Walen,[2] Chad D. Yuen,[2]
Patricia A. Thiel,[2,3,4] and James W. Evans[1,4]
[1]*Department of Physics & Astronomy, Iowa State University, Ames, Iowa 50011, USA*
[2]*Department of Chemistry, Iowa State University, Ames, Iowa 50011, USA*
[3]*Department of Materials Science & Engineering, Iowa State University, Ames, Iowa 50011, USA*
[4]*Ames Laboratory—USDOE, Iowa State University, Ames, Iowa 50011, USA*
(Received 20 February 2013; published 17 April 2013)

Scanning tunneling microscopy studies show that coarsening of arrays of rectangular single-layer Ag islands on Ag(110) at 220 K and below occurs by one-dimensional (1D) decay of narrower islands, which maintain roughly constant width in the ⟨001⟩ direction. Adatoms mainly detach from the island ends with ⟨001⟩ step edges. 1D decay derives from the absence of corner rounding diffusion from ⟨001⟩ to ⟨$\bar{1}$10⟩ edges and from inhibited nucleation of new layers on ⟨$\bar{1}$10⟩ edges. In contrast, rounding from ⟨$\bar{1}$10⟩ to ⟨001⟩ edges is active. The island decay rate exhibits an unexpectedly low effective Arrhenius energy due to a combination of strong anisotropy in terrace diffusion and a decrease with temperature of typical island end-to-end separations. Behavior is described by atomistic modeling, which accurately captures both the thermodynamics and the edge diffusion kinetics of the system, in contrast to previous treatments. Kinetic Monte Carlo (KMC) simulations assess model behavior and clarify the driving force for coarsening, as well as various detailed features of the 1D decay process. Refined "atom-tracking" KMC simulations for island configurations matching the experiment recover the experimentally observed island decay times and further elucidate spatial aspects of the transfer of adatoms between islands.

DOI: 10.1103/PhysRevB.87.155420 PACS number(s): 68.35.Fx, 66.30.Fq, 68.37.Ef, 68.55.−a

I. INTRODUCTION

There is broad interest in the coarsening of arrays of islands, clusters, or droplets in materials science and chemistry, both for three-dimensional (3D) clusters in bulk phases[1,2] and for two-dimensional (2D) or 3D clusters supported on surfaces.[3–5] The most common coarsening mechanism is Ostwald ripening (OR),[6] wherein smaller than average clusters shrink, transferring their atoms by diffusion to larger clusters. The overall coarsening process is driven by a reduction in the energy cost associated with broken bonds at the periphery of clusters; the preferential dissolution of smaller clusters reflects their higher chemical potential. Most bulk and surface systems analyzed to date have been isotropic. Typically, local equilibration of cluster shape is facile, so the individual clusters quickly achieve and maintain their equilibrium shapes during this coarsening process. For crystalline clusters, the equilibrium shape is determined according to the Wulff construction by the orientation-dependent edge energies for 2D clusters and surface energies for 3D clusters (as well as by the adhesion energy for the latter).

Submonolayer homoepitaxial films on face-centered cubic (fcc) metal surfaces provide ideal systems in which to perform fundamental analyses of the coarsening of arrays of single-atom-high 2D islands.[4,5] Fcc(111) and fcc(100) surfaces are isotropic. However, fcc(110) surfaces are anisotropic, providing the possibility to explore the effects of strong anisotropy in both surface diffusion and interactions between adatoms. Terrace diffusion on fcc(110) surfaces can be strongly anisotropic because the surface consists of an array of parallel channels in the ⟨$\bar{1}$10⟩ direction. In-channel hopping diffusion is typically more facile than cross-channel hopping in the ⟨001⟩ direction.[7] (One caveat is that cross-channel exchange diffusion could have a lower rate than cross-channel hopping and even a comparable rate to in-channel diffusion in some systems.) The rectangular surface unit cell ensures that separations, and thus interactions, between neighboring atoms depend on direction, with shorter separations and stronger interactions in the in-channel direction.

In this paper, we consider the Ag/Ag(110) system where terrace diffusion is anisotropic and 2D single atomic layer Ag islands have rectangular equilibrium shapes with an aspect ratio $R_{eq} \approx 3$.[8] This value of R_{eq} reflects the ratio of the in-channel to cross-channel interaction strength. In pioneering studies of anisotropic coarsening on a metal surface, Morgenstern *et al.*[8,9] showed that in the Ag/Ag(110) system above ∼220 K, classic terrace diffusion-limited OR occurs, during which islands maintain their equilibrium shape. However, at lower temperatures, they showed that there exists a remarkable one-dimensional (1D) decay regime in which islands shrink in length with constant width and in which the aspect ratio can even evolve away from its equilibrium value. We present a detailed analysis of this anomalous coarsening regime utilizing both scanning tunneling microscopy (STM) experiments and atomistic modeling combined with kinetic Monte Carlo (KMC) simulation.

Experimental details of our paper are presented in Sec. II. Ag islands are formed by physical vapor deposition of Ag on the Ag(110) surface. Consequently, some background and analysis for this island formation process are provided in Sec. III. In addition, we discuss equilibrium versus nonequilibrium island shapes. The basic experimental observations of, and the proposed mechanism for, 1D island decay are presented in Sec. IV. An enumeration of the distinct initial, intermediate, and final stages of decay and certain subtle features thereof are presented in Sec. V, as well as further discussion of decay kinetics. Our refined atomistic model for the Ag/Ag(110) system is described in Sec. VI, and key benchmark results from KMC simulation for this model are presented in Sec. VII. Comparison of model predictions,

using atom-tracking KMC simulation, with the experiment is provided in Sec. VIII. Additional discussion and a summary are provided in Sec. IX.

II. EXPERIMENTAL DETAILS

All experiments were performed in a stainless-steel ultra-high-vacuum (UHV) chamber with a base pressure of 1×10^{-10} Torr (1.33×10^{-8} Pa), equipped with a variable temperature STM (Omicron, Germany). The Ag(110) samples were cleaned by repeated cycles of Ar^+ sputtering (1 keV, $\sim 2\ \mu$A, 8–16 min) and annealing (625–670 K, 10 min).

With the sample actively cooled in the STM stage to 173–260 K, silver was deposited via an Omicron EFM3 UHV evaporator containing Ag (99.99% pure). The true temperature of the sample was within ± 5 K of the reported value and was held constant during each experiment. The Ag flux ranged from $(6.6\text{–}45) \times 10^{-3}$ monolayers (ML)/s. STM images of the resulting island distributions were collected using electrochemically etched W tips and cut Pt-Ir tips. The Ag coverage θ was determined from the fractional area of submonolayer islands assessed using WsXM software and ranged from $\sim$0.09 to 0.38 ML. After deposition, the surface was scanned to find a suitable terrace on which to monitor postdeposition island evolution. A sequence of images was then obtained at intervals of $\sim$100 s.

Even trace amounts of chalcogens (O, S) can dramatically modify nanocluster stability and coarsening in fcc metal homoepitaxial systems.[10] Thus, we also performed controlled studies in which we exposed the surface to O_2 (gas) to assess this possibility. However, we found no significant effect of oxygen on coarsening in the Ag/Ag(110) system, as discussed later. In our experiments, the sample was exposed to O_2 by backfilling the chamber with O_2 (gas) to the desired pressure through a leak valve while continuously pumping with an ion pump. Based on previous studies,[11] in the range 150–300 K, oxygen undergoes irreversible dissociative adsorption. Oxygen exposure is reported in Langmuir ($1\ \text{L} = 10^{-6}$ Torr s). The oxygen coverage was estimated from the exposure and the sticking coefficient S, where S decreases from $\sim$0.008 at 150 K to $\sim$0.003 at 300 K.[12]

III. BACKGROUND: AG/AG(110) ISLAND FORMATION AND EQUILIBRIUM

In Fig. 1, we show STM images of Ag island distributions on Ag(110) taken after deposition of Ag at various temperatures (T). Analysis of island shapes either during island formation via deposition or during postdeposition coarsening should naturally compare observations with equilibrium island shapes. Thus, we first describe these equilibrium shapes in Sec. III A. Then, in Sec. III B, we describe and further develop some key aspects of the theory of island formation in anisotropic systems.

A. Island equilibrium shapes

Consider a rectangular single-layer Ag island on Ag(110) with the linear dimension $L^{\parallel}$ ($L^{\perp}$) in the $\langle \bar{1}10 \rangle$ ($\langle 001 \rangle$)direction. (In this paper, the notation $\langle \bar{1}10 \rangle$ is used to denote the two directions $[\bar{1}10]$ and $[1\bar{1}0]$, and the notation

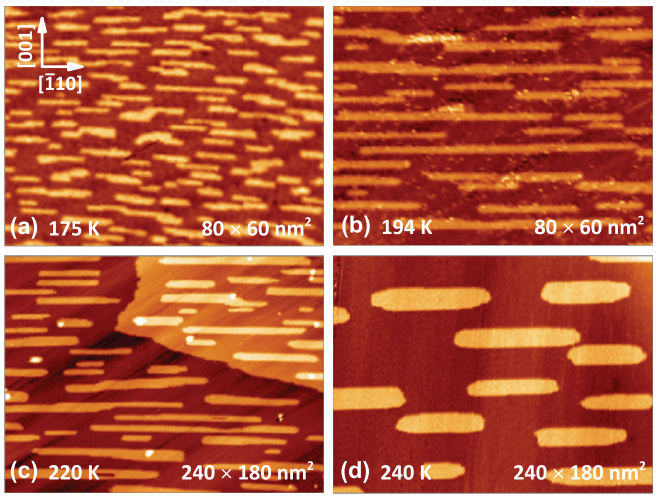

FIG. 1. (Color online) Ag island distributions on Ag(110) formed by deposition of Ag: (a) 175 K, 0.26 ML; (b) 194 K, 0.27 ML; (c) 220 K, 0.30 ML; and (d) 240 K, 0.23 ML. Images sizes are 80×60 nm^2 (top row) and 240×180 nm^2 (bottom row). Deposition flux is 0.02–0.04 ML/s.

$\langle 001 \rangle$ is used to denote the two directions [001] and $[00\bar{1}]$). The energy of the island can be written as

$$E_{\text{isl}} = \mu_\infty \Omega^{-1} A + 2(\gamma^{\parallel} L^{\parallel} + \gamma^{\perp} L^{\perp}), \tag{1}$$

with the island area $A = L^{\parallel} L^{\perp}$. Here, $\mu_\infty = \mu_{\text{ads}} + \mu_{\text{int}}$ is the chemical potential for an infinite island, where μ_{ads} is associated with the adsorption energy of isolated adatoms and μ_{int} is associated with the attractive lateral interactions. Also, $\Omega = 0.118$ nm^2 denotes the area of the surface unit cell, and $\gamma^{\parallel}$ ($\gamma^{\perp}$) denotes the step energy per unit length for steps aligned in the $\langle \bar{1}10 \rangle$ ($\langle 001 \rangle$) direction. Minimization of E_{isl} for a fixed A gives $\gamma^{\parallel} L^{\parallel}_{\text{eq}} = \gamma^{\perp} L^{\perp}_{\text{eq}}$, which shows that the equilibrium (eq) shape has an aspect ratio R equal to $R_{\text{eq}} = L^{\parallel}_{\text{eq}} / L^{\perp}_{\text{eq}} = \gamma^{\perp}/\gamma^{\parallel}$, where $R_{\text{eq}} \approx 3$ for Ag/Ag(110).[6] The chemical potential of a fully equilibrated island satisfies

$$\mu_{\text{isl}} = \Omega\, \mathrm{d}E_{\text{isl}}/\mathrm{d}A = \mu_\infty + 2\Omega\gamma^{\parallel}/L^{\perp} = \mu_\infty + 2\Omega\gamma^{\perp}/L^{\parallel}. \tag{2}$$

The chemical potential for an equilibrated dilute 2D adatom gas at the island edge has the form $\mu_{\text{gas}} = \mu_{\text{ads}} + k_{\text{B}}T \ln(n_{\text{eq}})$, where n_{eq} is the adatom density per site, and k_{B} is the Boltzmann constant. Since μ_{gas} must equal μ_{isl} at the island edges, it follows that the density of this 2D adatom gas equals $n_{\text{eq}} = n_\infty \exp(2\beta\Omega\gamma^{\parallel}/L^{\perp}) = n_\infty \exp(2\beta\Omega\gamma^{\perp}/L^{\parallel})$. Here, $\beta \equiv 1/(k_{\text{B}}T)$ denotes the inverse temperature, and $n_\infty = \exp(\beta\mu_{\text{int}})$ denotes the equilibrium adatom density at an extended straight step edge. Thus, smaller islands have higher n_{eq}, so conventional OR corresponds to net diffusion of adatoms between islands in the downhill direction with respect to adatom density. Later, we let $E_{\text{form}} = -\mu_{\text{int}} > 0$ denote the "formation energy" corresponding to the energy cost to form a 2D gas adatom by extraction of an adatom from a large 2D island.

B. Island formation

Terrace diffusion-limited coarsening is impacted by the spatial distribution of islands. In our studies, island distributions are created by deposition at various temperatures. Thus, we briefly describe key aspects of the theory of island formation with anisotropic terrace diffusion, which elucidate the spatial arrangement of islands. First, previous studies indicate that island formation is irreversible (in the sense that there is no significant in-channel bond breaking) up to 200–220 K.[13–15] This covers most of the regime of interest here, so we present results only for this case.

Let $h^{\parallel} = \nu \exp(-\beta E_d^{\parallel})$ [$h^{\perp} = \nu \exp(-\beta E_d^{\perp})$] denote the rate for hopping between adjacent sites in the $\langle \bar{1}10 \rangle$ in-channel ($\langle 001 \rangle$ cross-channel) direction, with prefactor $\nu \approx 10^{13}$/s and where $E_d^{\perp} = 0.38$eV and $E_d^{\parallel} = 0.28$eV for Ag/Ag(110).[13] It is convenient to introduce the quantity

$$r \equiv (h^{\parallel}/h^{\perp})^{1/2} = \exp[\beta(E_d^{\perp} - E_d^{\parallel})/2]. \quad (3)$$

Then, $r = \exp(0.05\beta)$ (here and later, β always has units of eV^{-1}) for Ag/Ag(110), which measures the strength of the terrace diffusion anisotropy. Previous theoretical analysis[16] reveals crossover behavior for the island density N_{isl} (measured per site) between (1) quasi-isotropic scaling $N_{isl} \sim (F/h_{av})^{\chi}$, with $\chi = 1/3$ and $h_{av} \equiv (h^{\parallel}h^{\perp})^{1/2}$ for $N_{isl} \ll r^{-1}$, and (2) 1D anisotropic scaling $N_{isl} \sim (F/h^{\parallel})^{\chi}$, with $\chi = 1/4$ for $N_{isl} \gg r^{-1}$.

For Ag/Ag(110), $N_{isl} \approx 10^{-2.6}$ versus $r^{-1} = 10^{-1.4}$ at 175 K and $N_{isl} \approx 10^{-3.8}$ versus $r^{-1} = 10^{-1.1}$ at 220 K. This analysis indicates quasi-isotropic scaling in the regime from 175–220 K, which is of interest in this paper, although previous simulations found χ somewhat below 1/3 at 200 K.[13]

To further characterize spatial aspects of the island distribution, it is instructive to regard the surface as being tessellated into anisotropic "capture zones" (CZs) surrounding each island, where atoms deposited within these CZs typically aggregate with the corresponding island.[7] These CZs have characteristic linear dimensions $L_{CZ}^{\parallel}$ ($L_{CZ}^{\perp}$) in the $\langle \bar{1}10 \rangle$ ($\langle 001 \rangle$) direction. See Fig. 2. (In this simplified picture, the CZ tessellation is regarded as a periodic tiling of rectangles.) Then, in the quasi-isotropic scaling regime, theoretical analysis also indicates that CZs have an aspect ratio of $\sim r$.[16] Thus,

$$\Omega/N_{isl} \sim L_{CZ}^{\parallel} L_{CZ}^{\perp} \approx A_{CZ} \text{ and } L_{CZ}^{\parallel}/L_{CZ}^{\perp} \sim r, \quad (4)$$

where A_{CZ} is the CZ area so that

$$L_{CZ}^{\parallel} \sim (\Omega r/N_{isl})^{1/2} \sim \Omega^{1/2} \exp[\beta(E_d^{\perp} - 2E_d^{\parallel})/6] \quad (5)$$

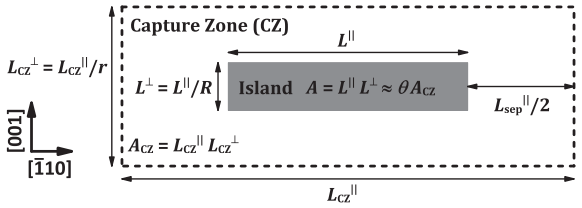

FIG. 2. Schematic showing Ag island and CZ geometry on Ag(110), together with various lengths and their relationships, as discussed in the text.

in the quasi-isotropic regime. Using $E_d^{\perp} = 0.38$ eV and $E_d^{\parallel} = 0.28$ eV for Ag/Ag(110), $L_{CZ}^{\parallel} \sim \exp(-0.03\beta)$, which exhibits a weak T dependence. This feature is roughly consistent with STM images of island arrays, at least for Ag deposition above 175 K. See Fig. 1.

In addition to anisotropic CZs, a key feature of the Ag/Ag(110) system is the formation of highly elongated rectangular Ag islands for deposition below ~240 K. Again, $L^{\parallel}$ ($L^{\perp}$) denotes the island dimension in the $\langle \bar{1}10 \rangle$ ($\langle 001 \rangle$) direction, so the island area equals $A \approx L^{\parallel}L^{\perp}$. See again Fig. 2. Then, the aspect ratios of islands formed by deposition usually satisfy $R = L^{\parallel}/L^{\perp} \gg R_{eq} \approx 3$. The feature $R \gg R_{eq}$ is due to anisotropic corner rounding: deposited adatoms, once reaching island edges, can go from the $\langle \bar{1}10 \rangle$ to the $\langle 001 \rangle$ side of the island on the timescale of deposition, but not the reverse.[17]

Of particular relevance for our analysis of 1D decay is an effective separation distance, L_{sep}, of the $\langle 001 \rangle$ ends of small, narrow islands to the end of the nearest island. This type of quantity has not been characterized. From a point in middle of the $\langle 001 \rangle$ end of the small island, we first determine components, $L_{sep}^{\parallel}$ ($L_{sep}^{\perp}$), in the $\langle \bar{1}10 \rangle$ ($\langle 001 \rangle$) directions of the separation to the $\langle 001 \rangle$ end of the nearest island. (We choose the point on the nearest island to be the closest point rather in the center of its end, because this distance may better reflect the extent of mass transfer.) Then, we define an effective separation L_{sep} to account for anisotropy in diffusion as

$$(L_{sep})^2 \equiv (L_{sep}^{\parallel})^2 + r^2(L_{sep}^{\perp})^2. \quad (6)$$

This definition of L_{sep} includes a penalty for the component of separation in the slow diffusion direction. However, for most cases considered, $L_{sep}^{\perp}$ is small or close to zero due to reasonably good alignment of islands with their neighbors so that $L_{sep} \approx L_{sep}^{\parallel}$.[18] We determine L_{sep} from STM images of island distributions after deposition, such as those in Fig. 1, obtaining values at each temperature for several smaller, narrower islands. Results are shown in Fig. 3. Significantly, this analysis indicates a T dependence with an effective Arrhenius energy of $E_{sep} \approx 0.2$ eV. L_{sep} is well defined after specifying that sampling occurs from islands smaller than a certain fraction (say, 1/3) of the average size and assuming that a large enough sample can be taken to precisely determine average behavior. However, there is a large spread in L_{sep} values for individual islands in the specified sample set (as illustrated in Fig. 3), so in practice there are large uncertainties due to our limited sampling of islands. Nonetheless, we believe that the trend in L_{sep} with varying T is clear and that our estimate of E_{sep} is reliable.

IV. OBSERVATIONS OF AND MECHANISM FOR 1D DECAY

A. Experiment

As is typical for coarsening studies, we monitor the decrease in the density N_{isl} (again, measured per site) for arrays of Ag islands on oxygen-free Ag(110). Instead, we could monitor an increase in average island size $s_{av} = \theta/N_{isl}$. We performed such studies for arrays of islands formed by deposition at various T ranging from 260 to 175 K, finding a rapid decrease

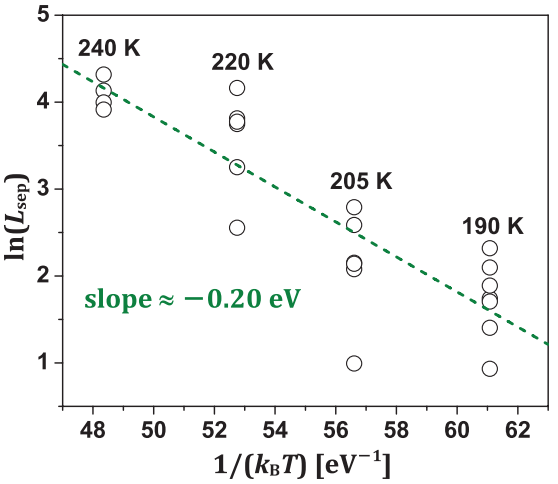

FIG. 3. (Color online) Arrhenius behavior of the effective island end-to-end separation distance $L_{sep} \sim \exp(-\beta E_{sep})$ with $E_{sep} \approx 0.20$ eV. For each T, several experimental data points are shown for L_{sep} (in nanometers) for individual smaller narrower islands, which are usually quite well aligned with their neighbors. The dashed line is a linear least-squares fit to the data points.

in N_{isl} at 260 K changing to a very slow decrease at 175 K (not shown). However, in these studies, the initial island size also varies with T. Since this size impacts the coarsening rate, we prefer analysis of the decay of individual islands in order to more systematically assess temperature effects and other significant factors. In related studies, we exposed an array of coarsening Ag islands to either 0.52 or 1 L of O_2 (gas) at 195 and 175 K and found no influence on the rate of decrease of N_{isl} after exposure. Figure 4 presents an example of results from such an experiment at 195 K, showing similar coarsening both prior to and after exposure to O_2.

Henceforth, we focus exclusively on analysis of the decay of individual small, narrow islands. Our analysis is motivated in part by the observations of Morgenstern *et al.*,[8] who found a crossover from conventional 2D decay to 1D decay as T decreases below $T_c \approx 220$ K, and a cessation of coarsening at $T_1 \approx 175$ K. Our own studies found 2D decay at 240 K and above and 1D decay at 220 K and below, with very slow 1D decay at 175 K. See Fig. 5, which shows behavior for 175, 190, and 220 K. While the T dependence that we observe is not in perfect agreement with that reported by Morgenstern *et al.*,[8] the differences are quite minor considering that these are results from two different laboratories (e.g., with some difference in temperature calibration naturally expected.) Also, our data at 220 K are limited, and our simulations suggest the possible onset of 2D decay. From the previous analysis of Morgenstern *et al.*[8] for 1D decay at lower T, the aspect ratio R can decrease below $R_{eq} \approx 3$, corresponding to evolution away from equilibrium shapes. However, the observations of Ref. 8 also revealed that the effective lower limit R_{min} is about unity. This implies that in the late stage of decay, there is a transition from 1D to 2D decay.

In Fig. 6, we summarize results for the T dependence of the decay rate dA/dt (in units of square nanometers per second) of small, narrower islands from 175–220 K. We estimate the decay rate dA/dt from a linear fit to the measured data. A value

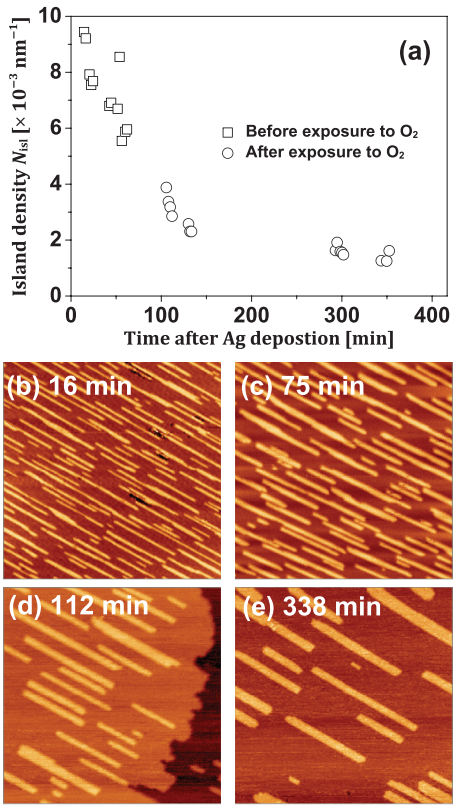

FIG. 4. (Color online) (a) Decrease of the island density N_{isl} during coarsening at 195 K. Initial coarsening for the clean Ag/Ag(110) system is shown (b) 16 min and (c) 75 min after deposition of Ag. See also open squares in (a). The system is exposed ~80 min to 1 L of O_2. Subsequent island configurations are shown (d) 112 min (i.e., ~32 min after O_2 exposure) and (e) 338 min (i.e., ~258 min after O_2 exposure). See also open circles in (a). O_2 exposure has no apparent effect on the decay of N_{isl}. Image sizes are 100 × 100 nm^2.

for the Arrhenius energy of $E_{OR} = -d[\ln(-dA/dt)]/d\beta \approx 0.32$ eV is obtained from this plot, which is much lower than the value for OR of Ag islands on the isotropic Ag(111) surface.[4] The data shown come from studies without and with oxygen (revealing no systematic difference in behavior) and include results from the studies of Morgenstern *et al.*[8,9] Analogous to Fig. 3, for each T there is a range of decay rates, because these depend on the local environment of selected islands and on relative island widths. However, this large data set unambiguously illustrates the trend in the average behavior of the decay rate with varying T.

B. Constrained thermodynamics for 1D decay

Traditional theories predict the absence of OR in pure 1D systems.[19] Thus, it is useful to first provide a framework to help understand behavior in the 1D decay regime for this strongly anisotropic quasi-1D Ag/Ag(110) system, where an additional complication is that island shapes are not equilibrated. We utilize the concept of a suitably defined partial chemical potential.[20,21] The partial chemical potential for ⟨001⟩ steps during 1D decay with constant $L^{\perp}$, where $dA = L^{\perp} dL^{\parallel}$ with fixed $L^{\perp}$, is given by

$$\mu_{001} = \Omega\, dE_{isl}/dA = \mu_{\infty} + 2\Omega\gamma^{\parallel}/L^{\perp}, \qquad (7)$$

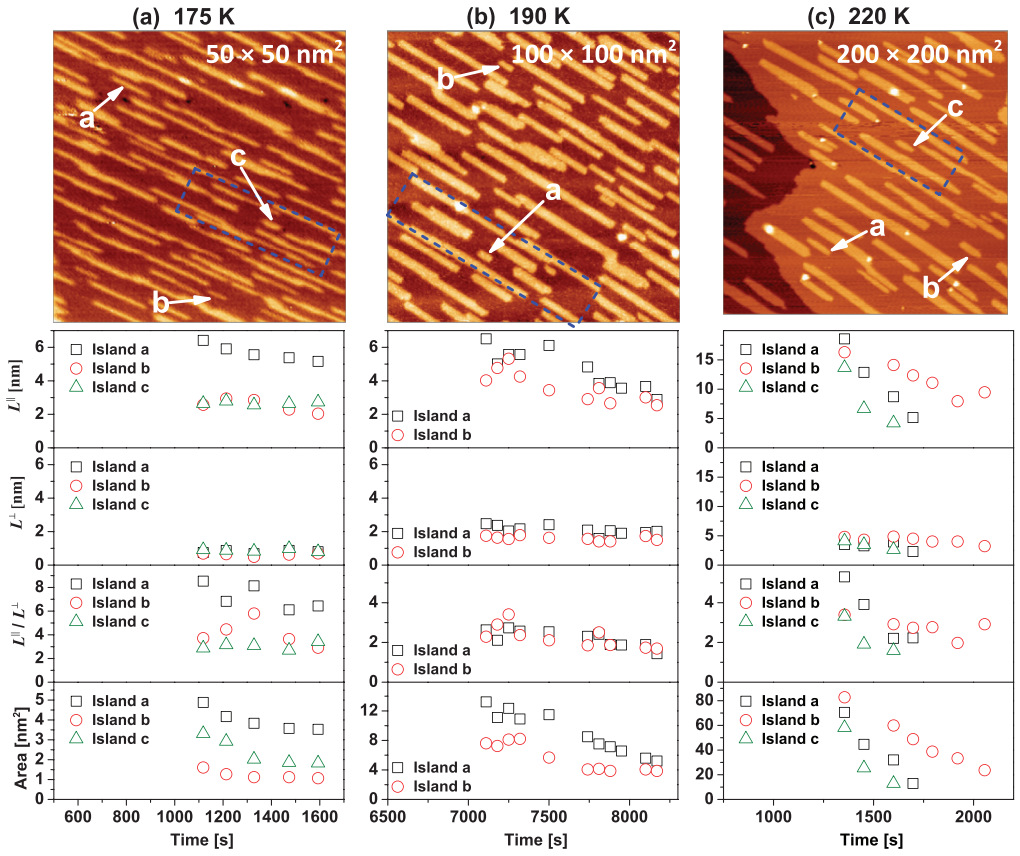

FIG. 5. (Color online) Analysis of STM data for the decay of individual islands at (a) 175 K (left column), (b) 190 K (middle column), and (c) 220 K (right column). Top row: STM images showing islands analyzed at the beginning of decay with image sizes: (a) 50 × 50 nm^2, (b) 100 × 100 nm^2, and (c) 200 × 200 nm^2. Second and third rows: Linear dimensions $L^{\parallel}$ ($L^{\perp}$) taken as caliper lengths in the $\langle\bar{1}10\rangle$ ($\langle 001\rangle$) directions. Fourth row: Island aspect ratios. Fifth row: Island areas. Outlined rectangular areas in the three STM images correspond to simulation cells for our atomistic modeling of island decay, described in later sections.

using Eq. (1) for $E_{\rm isl}$. The associated local equilibrium edge adatom density per site satisfies $n_{001} = n_{\infty}\exp(2\beta\Omega\gamma^{\parallel}/L^{\perp})$.[22] Thus, for 1D decay (with constant $L^{\perp}$), not all islands have the same chemical potential, in contrast to pure 1D coarsening models. As a result, narrower Ag islands on Ag(110) with higher μ_{001} shrink, while wider islands with smaller μ_{001} grow. This occurs by terrace diffusion-mediated transfer of adatoms from the $\langle 001\rangle$ ends of the narrower islands with higher n_{001} to those of the wider islands with lower n_{001}.

C. Kinetic mechanism for 1D decay

Morgenstern *et al.*[8] made several key observations regarding the kinetic mechanism underlying 1D decay. Detachment from kinks on $\langle\bar{1}10\rangle$ edges is only active above ∼220 K, because this involves difficult cross-channel diffusion and strong bond breaking. Likewise, corner rounding from $\langle 001\rangle$ edges to $\langle\bar{1}10\rangle$ edges is only active above ∼220 K, in contrast to the reverse process. However, in-channel detachment from $\langle 001\rangle$ edges is active above ∼170 K. Thus, net detachment of adatoms can occur from islands that are narrower than average (with smaller $L^{\perp}$), leading to growth of wider islands. This 1D decay also requires diffusion in the $\langle 001\rangle$ direction on the terrace in order for adatoms to sense the chemical potential differences between narrower and wider islands described earlier. Diffusion along $\langle 001\rangle$ edges is fairly inactive below ∼220 K.

V. DETAILED CHARACTERIZATION OF 1D DECAY

A. Stages of decay

It is instructive to distinguish three stages for 1D decay at 220 K and below, at least for a common situation in which the initial configuration is a highly elongated island. Detailed assessment of behavior in these regimes raises some issues regarding consistency with the kinetic mechanism presented in Sec. IV C. However, we resolve each of these issues here.

1. *Initial stage for highly elongated islands with $R > R_{\rm eq}$*

There is a thermodynamic driving force for island widening (i.e., an increase of $L^{\perp}$) when $R > R_{\rm eq}$. However, such widening is not observed during the decay process. This is perhaps surprising, since according to Sec. IV C, adatoms can detach from $\langle 001\rangle$ edges and diffuse in the cross-channel $\langle 001\rangle$ direction on terraces. Then, why do they not reattach at nearby $\langle\bar{1}10\rangle$ edges of the same island, causing island widening, versus attaching at more distant $\langle 001\rangle$ steps of other islands or extended step edges? Our proposed explanation is

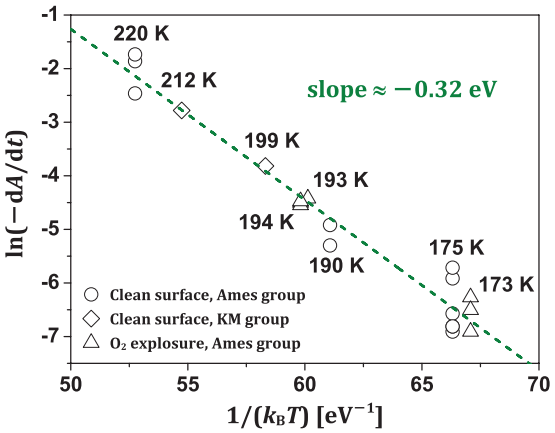

FIG. 6. (Color online) Arrhenius behavior of the island decay rate $-\mathrm{d}A/\mathrm{d}t$ (in units of square nanometers per second). Data are compiled from our studies (open circles) and Morgenstern *et al.* (Refs. 8 and 9) (KM, diamonds) for the clean Ag/Ag(110) system and from our studies for Ag/Ag(110) exposed to oxygen (open triangles). Initial sizes of decaying islands are 58, 71, and 83 nm^2 at 220 K; 93 nm^2 at 212 K (Ref. 9); 5.9 nm^2 at 199 K (Ref. 8; with rate determined from regime before 2D decay); 18, 39, and 45 nm^2 at 194 K; 8.1 nm^2 at 193 K; 7.6 and 13 nm^2 at 190 K; 1.6, 2.9, 3.3, 4.6, 4.9, and 5.8 nm^2 at 175 K; and 1.9, 3.7, and 4.1 nm^2 at 173 K. The dashed line is a linear least-squares fit to the experimental data with slope corresponding to an Arrhenius energy of $E_{\mathrm{OR}} \approx 0.32$ eV.

that such widening is nucleation limited, as new layers must be created by nucleation on the outer facetted $\langle \bar{1}10 \rangle$ edges. This nucleation process must occur too slowly on the timescale of island decay for it to be significant, an issue to which we return in Sec. VII.

2. *Intermediate stage with* $R_{\mathrm{eq}} < R \leqslant R_{\mathrm{min}} \approx 1$

In the intermediate stage, where R is decreasing below R_{eq}, island shapes are evolving further from equilibrium. Equilibration would correspond to island thinning (i.e., decreasing $L^{\perp}$) and increasing R. The lack of thinning is perhaps surprising, since adatoms can detach from the top and bottom rows on the $\langle \bar{1}10 \rangle$ edges and reattach to the $\langle 001 \rangle$ edges. However, this island thinning mechanism must be inefficient on the timescale of decay. It is plausible that the removal of adatoms from an entire $\langle \bar{1}10 \rangle$ edge is a slow process. Also, the free energy gain in transferring those atoms to the $\langle 001 \rangle$ edge is small, so the thermodynamic driving force for thinning is low when R is significantly above R_{min}.

3. *Late-stage decay for* $R < R_{\mathrm{min}}$

As R approaches $R_{\mathrm{min}} \approx 1$, the local chemical potential of the $\langle \bar{1}10 \rangle$ edge significantly exceeds that of the $\langle 001 \rangle$ edge, and the timescale of removal of entire $\langle \bar{1}10 \rangle$ edges becomes shorter. Thus, transfer from $\langle \bar{1}10 \rangle$ to $\langle 001 \rangle$ edges becomes sufficiently facile to block further decrease of R. This feature is nicely demonstrated in the data shown in fig. 2(a) of Morgenstern *et al.*[8] Since now both edge lengths decrease with roughly fixed R, the excess chemical potential of a finite island increases like $1/L^{\parallel} \sim 1/L^{\perp}$. Thus, we should recover classic terrace diffusion-limited scaling of island area $A \sim (t_0 - t)^{2/3}$ as for in isotropic systems, where t_0 is the time of island disappearance.[4,5]

B. Variation of decay rate with time

Suppose that diffusion-limited 1D decay occurs with no significant attachment or detachment from $\langle \bar{1}10 \rangle$ edges (at least prior to reaching the late-stage decay regime). Then, to a first approximation, since $L^{\perp}$ is constant, the decay rate should also be constant. In a refined assessment, the rate should slowly decrease as the separation L_{sep} between the $\langle 001 \rangle$ end of the decaying island and the $\langle 001 \rangle$ ends of its neighbors increases. The data in Fig. 5 seem consistent with this perspective, but other factors can be operative, as described later.

Fits to previous data for 1D decay at 200 K were based on a perceived rate increase during decay.[8,23] The explanation of Morgenstern *et al.*[8] for this rate increase was based on the assumed occurrence of significant recondensation of adatoms detaching from $\langle 001 \rangle$ edges onto $\langle \bar{1}10 \rangle$ edges of the same island, followed by edge transport back to the $\langle 001 \rangle$ edge. The overall effect of these processes is to slow decay. However, as $L^{\parallel}$ decreases, the extent of recondensation should become less significant, resulting in a faster decay rate. This picture should apply for facile transport of edge adatoms from $\langle \bar{1}10 \rangle$ to $\langle 001 \rangle$ edges. One caveat is that if instead this transport is corner rounding limited, then the rate of feeding adatoms back to the $\langle 001 \rangle$ edge due to recondensation should be independent of island length. In this case, the island decay rate should be constant or slowly decreasing, as discussed earlier. However, for a realistic atomistic model (cf. Sec. VI), it is plausible that transport is not corner rounding limited. Then, the picture of Morgenstern *et al.*[8] for an increase in decay rate is viable, although it is difficult to assess the magnitude of this effect.

Previous analysis of 1D decay adopted the scaling form $A \sim (t_0 - t)^x$. The theoretical treatment of Yao *et al.*[23] claimed that $x = 1/2$. Morgenstern *et al.*[8] fit experimental data using $x = 2/3$, although it is not clear why their recondensation picture would produce an exponent. We offer two cautions regarding fitting of area decay to such a simple scaling form. First, this single simple scaling form was used to simultaneously fit both regime 2 and the late-stage regime 3, where $x = 2/3$. This would force values of $x < 1$ even for perfectly linear decay in regime 2. Second, we claim that there are significant fluctuations in the decay process, which can conceal typical or average behavior. The extent of fluctuations is most readily demonstrated in simulations, where we can rerun the stochastic decay process for the same initial island configuration. See Secs. VII and VIII.

C. Arrhenius behavior

For 2D isotropic terrace diffusion-limited decay, classic treatments show that the shrinking area of islands that are much smaller than average satisfies[4,5]

$$\mathrm{d}A/\mathrm{d}t \sim -Dn_{\infty}\gamma/[A^{1/2}\ln(\langle A_{\mathrm{CZ}}\rangle/\langle A\rangle)], \qquad (8)$$

where $D = D_0 \exp(-\beta E_{\mathrm{d}})$ is the terrace diffusion coefficient and E_{d} is the corresponding activation barrier, $n_{\infty} = \exp(-\beta E_{\mathrm{form}})$ as in Sec. III A, γ is the step energy, and $\langle A_{\mathrm{CZ}}\rangle$ ($\langle A\rangle$) is the average CZ area (island area). Here, $\langle A_{\mathrm{CZ}}\rangle / \langle A\rangle$ can be replaced by the square of the ratio of

the island separation to island linear dimension. However, since the dependence on island separation is logarithmic, the T dependence of this quantity does not contribute to the Arrhenius energy for isotropic terrace diffusion-limited OR of $E_{OR} = -d[\ln(-dA/dt)]/d\beta = E_d + E_{form}$.[24]

For 1D decay with strongly anisotropic terrace diffusion, solution of a quasi-1D diffusion problem for the flux from narrow to broader islands suggests the form

$$dA/dt \sim -D^{\parallel} n_{\infty} \gamma^{\parallel} L^{\perp}(1/L^{\perp} - 1\langle L^{\perp}\rangle)/L_{sep}, \qquad (9)$$

where $D^{\parallel} = D_0^{\parallel} \exp(-\beta E_d^{\parallel})$ is the fast in-channel diffusion rate, $n_{\infty} = \exp(-\beta E_{form})$, and $L_{sep} \sim \exp(-\beta E_{sep})$ is the distance from the $\langle 001\rangle$ end of the decaying island to that of the closest island (cf. Sec. III B). The "strong" dependence on L_{sep} for quasi-1D coarsening (versus the weak logarithmic dependence on island separation for isotropic coarsening) implies that the T dependence of L_{sep} impacts the Arrhenius energy

$$E_{OR} = -d[\ln(-dA/dt)]/d\beta = E_d^{\parallel} + E_{form} - E_{sep}, \quad (10)$$

for 1D decay. For our model described in Sec. VI, we have $E_d^{\parallel} = 0.28$ eV and $E_{form} = 0.225$ eV, and from Sec. III, we have $E_{sep} \approx 0.20$ eV. As a result, it follows that $E_{OR} \approx 0.31$ eV, which is consistent with the experimental behavior in Fig. 6.

VI. ATOMISTIC MODEL FOR AG/AG(110) CAPTURING BOTH THERMODYNAMICS AND KINETICS

Extensive modeling of island formation during deposition for the Ag/Ag(110) system has been performed using a lattice-gas model incorporating a standard bond-breaking or initial value approximation (IVA) formulation of activation barriers for intralayer adatom hopping on the Ag(110) surface.[13,25] Hopping of isolated adatoms is described by a low in-channel barrier of $E_d^{\parallel} = 0.28$ eV for the $\langle \bar{1}10\rangle$ direction and a higher cross-channel barrier of $E_d^{\perp} = 0.38$ eV for the $\langle 001\rangle$ direction. IVA barriers for edge diffusion and detachment are boosted from the isolated adatom barriers by the strength of bonds in the initial state before hopping. In this IVA modeling, nearest-neighbor (NN) attractive interactions are adopted with the strength $E_b^{\perp} = -0.02$ eV for the cross-channel direction and $E_b^{\parallel} = -0.18$ eV for the in-channel direction. (The cross-channel NN separation equals $a = 0.409$ nm, the lattice constant of Ag, and the in-channel NN separation equals $b = a/\sqrt{2} = 0.289$ nm.) The model has been applied primarily to describe island formation during deposition but could also be applied to treat postdeposition evolution.[26]

While this selection of IVA model parameters reasonably captures edge diffusion barriers, it fails to describe the equilibrium island shape. Since step energies satisfy the relations $\gamma^{\perp} = (1/2)|E_b^{\parallel}|/b$, and $\gamma^{\parallel} = (1/2)|E_b^{\perp}|/a$, the model predicts that $R_{eq} \approx 6.4$ versus the experimental value of $R_{eq} \approx 2.9$.[6] Thus, the preceding model is not so appropriate for analysis of equilibration phenomena such as coarsening.

Simulation studies of decay of Ag islands on Ag(110) were performed in Ref. 9 using an atomistic model crafted to capture the rates and barriers for various edge diffusion processes, as determined from a semiempirical theory. Accurate description

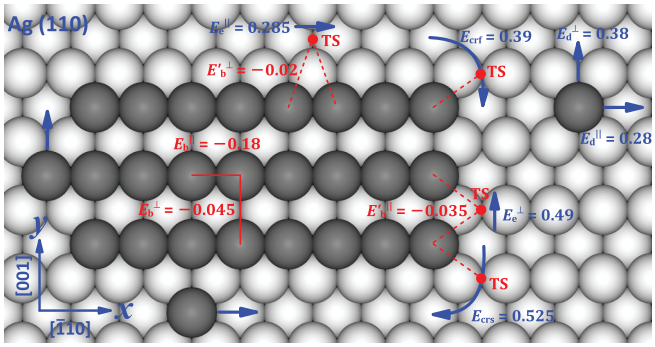

FIG. 7. (Color online) Schematic of our "refined" msLG atomistic model. NN interactions (red solid lines), unconventional interactions (red dashed lines), and edge diffusion barriers are shown (in eV). Two edge adatoms are shown at preferred adsorption sites, and the four red dots denote the locations of adatoms at various TSs. Edge barriers are $E_e^{\parallel} = E_d^{\parallel} + 2E'^{\perp}_b - E_b^{\perp}$ ($E_e^{\perp} = E_d^{\perp} + 2E'^{\parallel}_b - E_b^{\parallel}$) for straight $\langle \bar{1}10\rangle$ ($\langle 001\rangle$) edges. Corner rounding barriers are $E_{crf} = E_d^{\perp} + E'^{\parallel}_b - E_b^{\perp}$ ($E_{crs} = E_d^{\perp} + E'^{\parallel}_b - E_b^{\parallel}$) for fast (slow) rounding from the $\langle \bar{1}10\rangle$ to the $\langle 001\rangle$ edge (from the $\langle 001\rangle$ to the $\langle \bar{1}10\rangle$ edge).

of edge diffusion is appropriate given the lack of equilibration of islands shapes, which in turn implies that evolution is sensitive to the details of such kinetics. However, this modeling does not accurately describe equilibrium shapes as simulations evolve R to $R_{eq} \approx 5$ (Ref. 9) versus the experimental value of $R_{eq} \approx 2.9$.

Given the preceding shortcomings, a key requirement is to develop a model that simultaneously describes edge diffusion and detachment kinetics, as well as equilibrium island shapes. To this end, we adopt a recently developed multisite lattice-gas (msLG) model formulation.[27–29] In this class of models, we specify adsorption energies for adatoms at the energetically preferred adsorption sites in the troughs and at the two types of bridge sites corresponding to the transition states (TSs) for in-channel and cross-channel hopping. We also specify a set of "conventional" pairwise interactions between adatoms on nearby adsorption sites ($E_b^{\parallel}$ and $E_b^{\perp}$ in Fig. 7). In addition, we specify as second set of "unconventional" pairwise interactions between one adatom at a bridge site TS and another adatom at a nearby energetically preferred adsorption site ($E'^{\parallel}_b$ and $E'^{\perp}_b$ in Fig. 7). This second unconventional set of interactions is zero in IVA models. Allowing nonzero values in our msLG model provides additional flexibility and accuracy. The total energy E_i in the initial state before hopping and the total energy E_{TS} in the TS can be determined as the sum of the relevant adsorption energy and all relevant pairwise interactions. Then, the activation barrier for hopping is simply determined as $E_{act} = E_{TS} - E_i$. Hop rates are described by an Arrhenius form, $h = \nu \exp(-\beta E_{act})$, with the common prefactor $\nu = 10^{13}$/s. Processes are implemented with probabilities proportional to their rates in KMC simulations.

We chose adsorption energies to recover $E_d^{\parallel} = 0.28$ eV and $E_d^{\perp} = 0.38$ eV as in the IVA model. We include just two NN interactions with adatoms on NN adsorption sites $E_b^{\parallel} = -0.18$ eV and $E_b^{\perp} = -0.045$ eV. This produces an equilibrium island aspect ratio of $R_{eq} = 2.83$. We also include two "unconventional" interactions, with one adatom at an

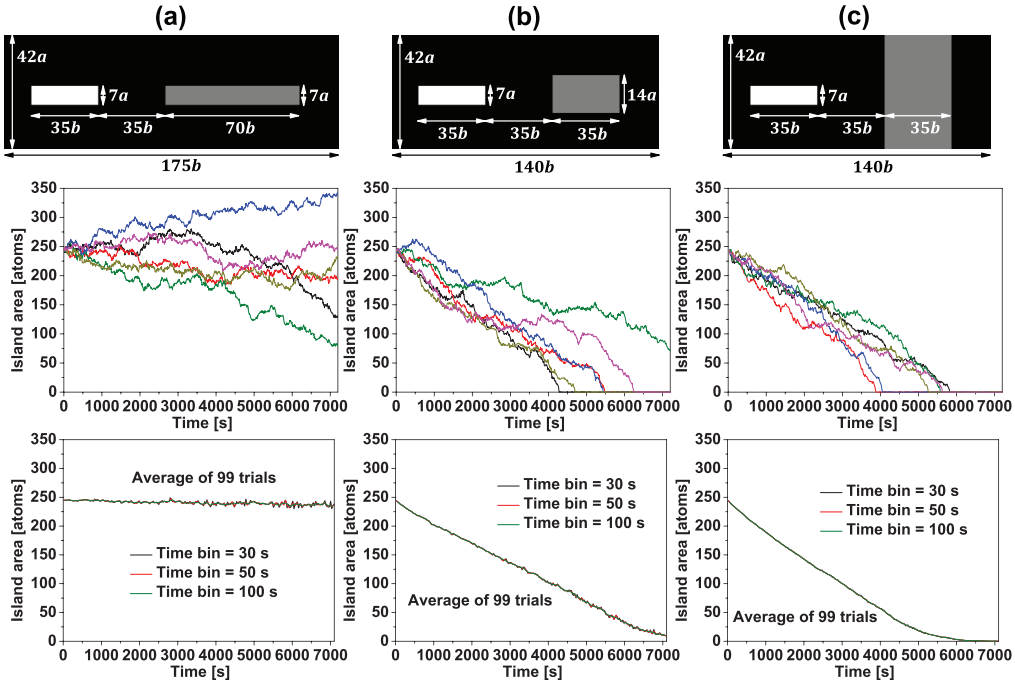

FIG. 8. (Color online) KMC simulations of our msLG model at 190 K assessing the thermodynamic driving force for island decay. Benchmark studies with two islands in the simulation cell: (a) equal width islands (left column), (b) unequal widths (middle column), and (c) an island–strip configuration (right column). The cell width is (a) 175b and (b) and (c) 140b. The initial configuration (with the decaying island in white) is shown on the top row. Results of six simulation trials are shown by differently colored curves in the middle row. Behavior averaging more than 99 trials is shown in the bottom row. Areas for individual trials are averaged over narrow bins (i.e., short time intervals), and values for each bin are averaged over trials. Similar results for different bin sizes are shown.

adsorption site and the other at a bridge site TS. See Fig. 7. These interactions are selected to reasonably recover values for edge diffusion and corner rounding rates as determined from direct energetic analysis (cf. Ref. 8). For example, the barrier for rounding from the $\langle\bar{1}10\rangle$ to the $\langle 001\rangle$ edge is $E_{\rm act} \approx 0.39$ eV, implying that this process is active over the T range of interest here. See again Fig. 7. Finally, the above msLG model still corresponds to an idealization of the actual diffusional dynamics of the system. It has been suggested that the actual path for transport in the $\langle 001\rangle$ direction involves exchange rather than hopping.[30] However, as long as the hopping barriers in our model produce reasonable rates for transport in this direction, model predictions should be reliable.

VII. BENCHMARK SIMULATIONS OF OUR ATOMISTIC MODEL FOR AG/AG(110)

It is instructive to perform tailored benchmark simulations to confirm some of the key ideas proposed in previous sections. In all analyses that follow, the island decay rate dA/dt is determine from the ratio of the initial area A_0 to the disappearance time t_0.

First, we examine the proposal that a difference in the widths of islands produces the thermodynamic driving force for 1D coarsening and thus controls the island decay rate. Specifically, we consider the decay of a small, narrow island in the presence of one other island in a "small" simulation cell with periodic boundary conditions. If the other island is twice as long with the same width, there is little decay and evolution is fluctuation dominated (Fig. 8(a)). If it is twice as wide but with the same length (thus having the same area as in Fig. 8(a)), there is significant decay (Fig. 8(b)). If the second island is a broader strip, decay is significantly faster (Fig. 8(c)). These differences are clearest in the average behavior shown in the bottom row. All of these observations are consistent with our constrained thermodynamic analysis in Sec. IV B.

Second, we assess our proposal of strong inhibition of the nucleation of new layers on $\langle\bar{1}10\rangle$ edges. Recall that this nucleation–inhibition blocks widening of highly elongated islands with $R > R_{\rm eq}$. See Sec. V A1. To this end, we add a chain of $N_{\rm chain}$ atoms on the facetted $\langle\bar{1}10\rangle$ edge of a small, narrow island and assess the fate of this chain (growth versus decay and disappearance) as a function of size $N_{\rm chain}$. Specifically, we consider the probability of growth of this chain $P_{\rm grow}$ as a function of $N_{\rm chain}$. Since it is difficult to identify the ultimate fate of the chain (e.g., because decaying chains can be very long lived), we run simulations for a specified time interval of length $t_{\rm max}$ and assign the outcome as growth if the chain survives. Figure 9 shows the results for a configuration with a small, narrow island and strip separated by $L_{\rm sep} = 35b$ and $70b$ in the simulation cell with periodic boundary conditions (similar to Fig. 8(c)), with $t_{\rm max} = 100$ s. The results do not change significantly when choosing $t_{\rm max} = 50$ s. It is convenient to define the critical chain size $N_{\rm crit}$ for nucleation by $P_{\rm grow}(N_{\rm crit}) = 0.5$. With this criterion, the behavior in Fig. 9 corresponds to a "large" value of $N_{\rm crit} \approx 4$; i.e., nucleation is strongly inhibited. A simple mean-field analysis of nucleation suggests that $P_{\rm grow} \sim (N_{\rm chain}/N^{\parallel})^{N_{\rm crit}}$

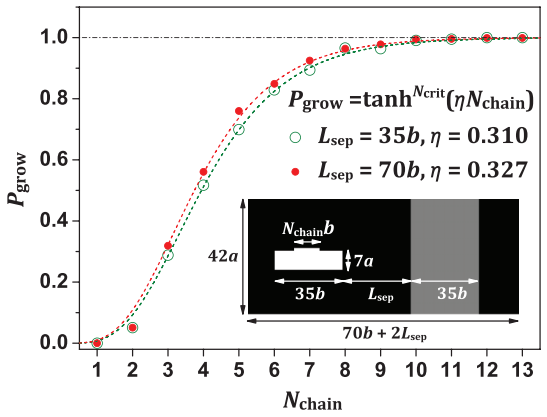

FIG. 9. (Color online) Growth probability for chains of atoms on a perfect $\langle \bar{1}10 \rangle$ island edge versus chain size (used to estimate N_{crit}) using $t_{max} = 100$ s. Simulations are performed at 190 K in a cell containing one narrow island and a strip (with initial configuration shown in the inset). Fitting using $P_{grow} = \tanh^{N_{crit}}(\eta N_{chain})$ is also shown by the dashed curves for $L_{sep} = 35b$ and $70b$.

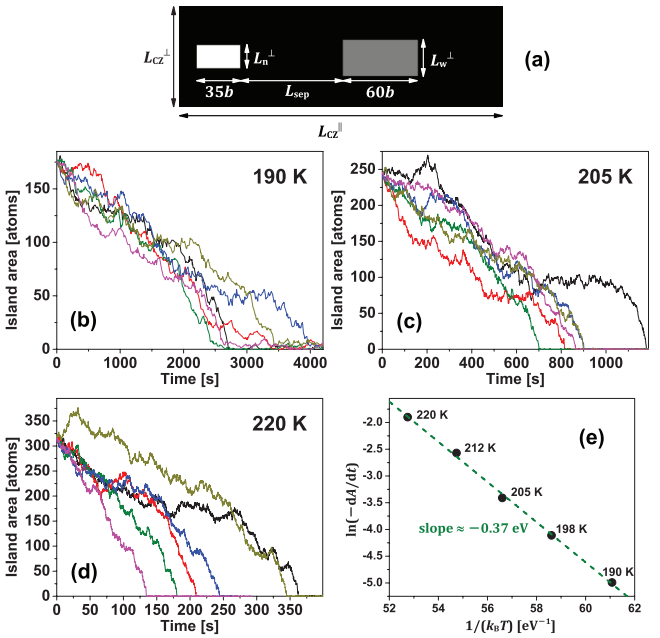

FIG. 10. (Color online) Benchmark simulations for the T dependence of the island decay rate: (a) simulation cell with a narrow (n) decaying island (white) and a wider (w) island (gray), where $L_{CZ}^{\parallel} = 95b + 2L_{sep}$. Simulation results are shown for (b) 190 K, (c) 205 K, and (d) 220 K. Parameters are $L_n^{\perp} = 5a$, $6a$, $7a$, $8a$, and $9a$; $L_w^{\perp} = 8a$, 9-$10a$ (averaging behavior), $11a$, 12-$13a$ (averaging behavior), and $14a$; $L_{sep} = 18b$, $28b$, $41b$, $57b$, and $82b$; and $L_{CZ}^{\perp} = 12a$, $15a$, $18a$, $27a$, and $39a$ for $T = 190$, 198, 205, 212, and 220 K, respectively. Simulation results are not shown for 198 and 212 K. (e) Arrhenius plot of the island decay rate with $E_{OR} \approx 0.37$ eV from a linear least-squares fit (dashed line).

for $N_{chain} \ll N^{\parallel} = L^{\parallel}/b$. Consistently, we find a reasonable fit to the overall growth probability behavior using the form $P_{grow} = \tanh^{N_{crit}}(\eta N_{chain})$ after suitable choice of the fitting parameter η.

The magnitude of N_{crit} depends on various features of the local geometry. For example, if we increase L_{sep} in a configuration like that of Fig. 9, then N_{crit} should decrease, as nucleation presumably becomes easier when the adatom sink with lower chemical potential is more distant. We find that doubling L_{sep} from the value of $35b$ to that of $70b$ slightly decreases N_{crit}. See Fig. 9. Likewise, N_{crit} would be somewhat affected by replacing the strip by a finite width island or by varying the length of the $\langle \bar{1}10 \rangle$ side of the decaying island.

Third, to explore the typical variation of island decay rate with time, we consider the simple island–island or island–strip configurations of Figs. 8(b) and 8(c). Results shown in the bottom row of Fig. 8, which average over many simulation trials, reveal no increase in the island decay rate and perhaps suggest a slight reduction. However, there are caveats. First, the strip configuration maximizes increase of L_{sep} during decay and thus the associated decrease of the decay rate. Second, the "tail" of averaged island decay curve must bend up, because the averaged area cannot vanish at any finite time (given that there is a finite probability of survival of the decaying island); from this perspective, it is appropriate to focus on the first part of the curves in the bottom row of Fig. 8. However, the final caveat is that initial transients could exist due to our choice of an initial perfect rectangular island. Given these caveats, it is possible that for other conditions, the decay rate could increase during island decay due to recondensation, as discussed in Sec. V B.

Fourth, we analyze the T dependence of decay, which we claim is strongly impacted by the T dependence of L_{sep}. For such an analysis, it is most instructive to explore behavior for simpler controlled island configurations. However, care must be taken in choosing the local island geometry to reasonably reflect typical experimental situations. In Fig. 10, we consider a configuration with two islands in a simulation cell with periodic boundary conditions where the small, narrow decaying island is aligned with a nearby broader larger island (typical of experiments). We perform simulations at five temperatures (190–220 K), adjusting the width of the smaller island to be consistent with typical narrower experimental islands. The width of the other island is always selected to be ∼60% larger. We select dimensions of the simulation cell so that its area increases with T similar to the experimental $A_{CZ} \approx \Omega/N_{isl}$. Significantly, we also select $L_{sep} \sim 82b \exp[-E_{sep}(\beta - \beta_{220K})]$ with $E_{sep} = 0.18$ eV to exhibit a simple Arrhenius dependence mimicking experiments. The results shown in Fig. 11 reveal a low effective Arrhenius energy, $E_{OR} \approx 0.37$ eV for the island decay rate, slightly above but similar to behavior in experiments.

We performed several additional analyses, varying the local island geometry to assess how this affects E_{OR}. If we repeat the preceding simulations but change just the geometry to misalign the broader island and the decaying island in the simulation cell with periodic boundary conditions, then the effective Arrhenius energy increases significantly to $E_{OR} \approx$ 0.41 eV. Also, fluctuations in the decay time are much greater for misaligned islands than for aligned islands, particularly at lower T. Similarly, replacing the broader island with a strip yields an even higher $E_{OR} \approx 0.44$ eV. From these additional analyses, we deduce that alignment of narrower islands in the direction of fast terrace diffusion is an important factor in producing an effective 1D system, as described by Eqs. (9)

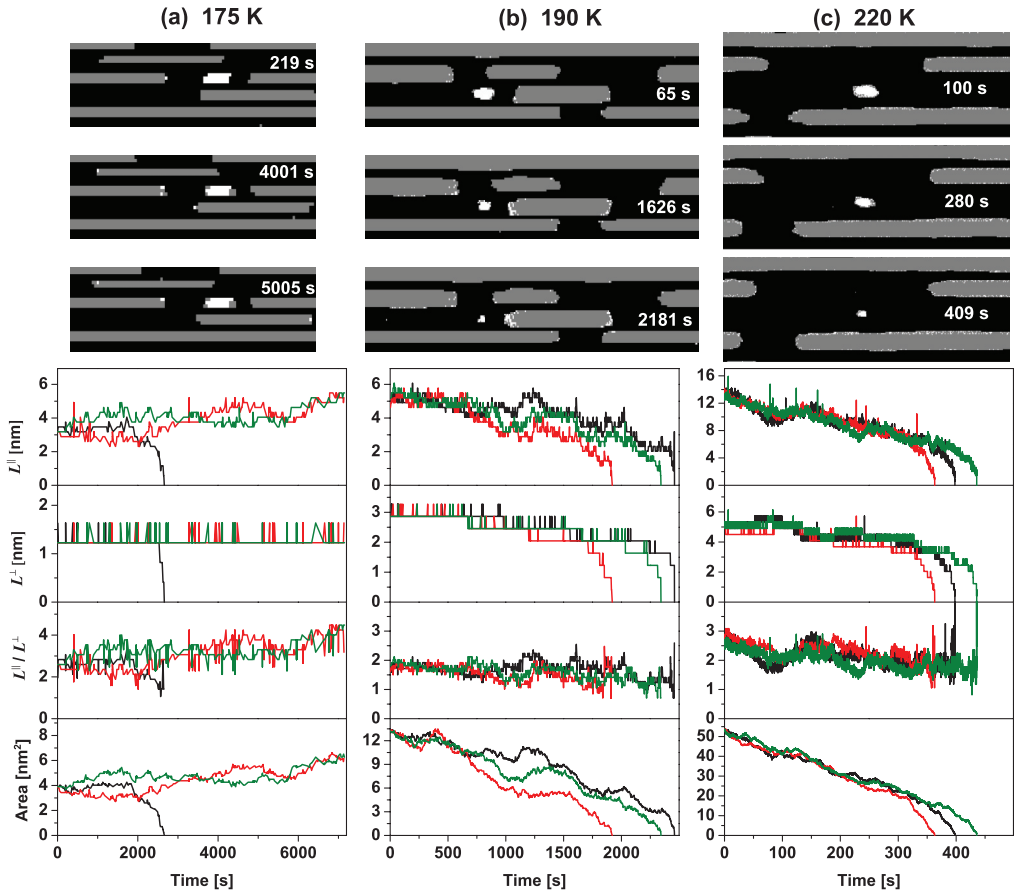

FIG. 11. (Color online) Atom-tracking KMC simulations of island decay for configurations mimicking those in the experimental images of Fig. 5: (a) tracks island c in Fig. 5(a) at 175 K (left column), (b) tracks island a in Fig. 5(b) at 190 K (middle column), and (c) tracks island c in Fig. 5(c) at 220 K (right column). Three simulation trials are shown in each case as differently colored curves. Top three rows: Simulated evolution during island decay. Snapshots with times shown are taken from the simulation trials corresponding to the green curves. Fourth row: Island length $L^{\parallel}$ in the $\langle\bar{1}10\rangle$ direction. Fifth row: Island width $L^{\perp}$ in the $\langle 001\rangle$ direction. Sixth row: Island aspect ratio. Seventh row: Island area. Dimensions of simulation cells are roughly (a) 30 $\times$ 10 nm^2, (b) 80 $\times$ 20 nm^2, and (c) 110 $\times$ 40 nm^2.

and (10), with low E_{OR}. This behavior might be anticipated from an appropriate continuum diffusion equation analysis (cf. Sec. IX).

VIII. COMPARISON OF KMC RESULTS FOR AN ATOMISTIC MODEL WITH THE EXPERIMENT

For the most direct comparison with the experiment, we perform simulations where the initial island configuration mimics the experimental configurations as determined from the STM analyses of island decay in Fig. 5. Our simulation cells are constrained to have periodic boundary conditions (in contrast to the experiment), but a judicious choice of cell location allows reasonable mimicking of the experimental environment of the decaying island with a moderate-size simulation cell. Compare Figs. 3 and 11. There are two significant advantages to performing such simulations. First, in contrast to the experiment, for a specific initial configuration, we can perform multiple simulations of stochastic evolution to assess the extent of fluctuations in these processes. By averaging over multiple simulations, we can obtain an accurate picture of typical behavior. Fluctuations can be significant, so a single simulation or experiment can give a misleading impression of behavior. Second, we can perform atom-tracking KMC simulations in which we label the adatoms in the narrow decaying island of interest and thereby assess where these atoms go after detachment (mainly from $\langle 001\rangle$ edges) and attachment to other edges.

Our results are shown in Fig. 11 for decay at three temperatures (175, 190, and 220 K) for island configurations extracted from Fig. 5. Refer to the supplemental material (Ref. 31) for corresponding movies. At 175 K, decay is marginal or very slow and fluctuation dominated, reflecting in part similar island widths of the decaying and nearby islands. At 190 K, decay is faster and more deterministic, with the selected island disappearing after $\sim$2000 s, consistent with the experiment. The island aspect ratio decreases slightly from $R \approx 2$ to $R \approx 1.5$, as in the experiment. Most adatoms detaching from the decaying island attach at the $\langle 001\rangle$ end of the closest aligned island. (The use of periodic boundary conditions for the simulation cell means that some adatoms "artificially" attach at the far end of this island.) At 220 K, decay is even faster, with the island disappearing after $\sim$400 s (similar to 300–400 s in

the experiment), and the aspect ratio decreases more strongly from $R \approx 3$ to around $R \approx 2$ or below (at least transiently), as in the experiment. Terrace diffusion is less anisotropic than at 190 K, and adatoms from the decaying island attach at various nearby island edges.

IX. DISCUSSION AND SUMMARY

STM studies provide a detailed characterization of the coarsening of arrays of rectangular single-layer Ag islands on Ag(110) and demonstrate that this process occurs primarily by 1D decay of narrower islands, maintaining roughly constant $L^{\perp}$ of ∼220 K and below. These observations are consistent with those of Morgenstern *et al.*,[8] who proposed that adatoms mainly detach from the ⟨001⟩ ends of islands and that corner rounding of edge adatoms from ⟨001⟩ to ⟨$\bar{1}$10⟩ edges is inactive. However, it is also the case that adatoms can diffuse in the cross-channel ⟨001⟩ direction on terraces; thus, there can be significant recondensation of atoms detaching from ⟨001⟩ steps onto ⟨$\bar{1}$10⟩ steps of the same island. Consequently, the lack of widening of highly elongated islands must also reflect the limited nucleation of new outer edges. Our studies also reveal an unexpectedly low effective Arrhenius energy for the decay rate, which we claim derives from a strong anisotropy in terrace diffusion, together with a reduction of the island ⟨001⟩ end separation L_{sep} with decreasing T. In addition, our paper and analyses address and clarify other basic aspects of 1D decay, such as the thermodynamic driving force and the detailed decay kinetics. We argue that the latter does not satisfy the scaling laws proposed previously.

Experimentally observed behavior was captured by KMC simulation analysis of a msLG atomistic model, which has the flexibility to accurately describe both thermodynamics and kinetics of the system. KMC studies with simple island configurations also clarify the thermodynamic driving force for coarsening and various other details of the 1D decay process. An appealing feature of our KMC studies is the capability to both input experimental island configurations and label adatoms in a specific decaying island in order to track spatial aspects of their transfer between islands.

In addition to KMC simulation studies of atomistic models, it is instructive to assess how traditional Burton–Cabrera–Frank (BCF)-type formulations of step dynamics[32] must be modified to treat 1D island decay processes during anisotropic coarsening. These treatments solve a boundary value problem for the steady-state anisotropic terrace diffusion equation with appropriate boundary conditions at island edges. For terrace diffusion limited decay, usually Dirichlet boundary conditions are applied, equating the adatom density to the appropriate equilibrium values at island edges. Complications arise for 1D decay, since island shapes are not equilibrated. We could exploit concepts of partial chemical potentials and local equilibrium densities for different edges (cf. Sec. IV B and Ref. 23). However, this is not sufficient to produce true 1D decay. Despite the absence of an energy barrier for attachment at steps, we claim that there is a large effective barrier to attachment to ⟨$\bar{1}$10⟩ steps and that we should use a correspondingly small effective Chernov kinetic coefficient.[33] This proposal reflects the feature that true attachment at steps requires incorporation at kink sites[33] and that these kink sites are rare on ⟨$\bar{1}$10⟩ steps. A treatment with a large effective barrier or correspondingly low effective kinetic coefficient for ⟨$\bar{1}$10⟩ steps will certainly capture 1D decay.

Going beyond simply refining the kinetic coefficients in Chernov-type boundary conditions within a BCF-type formalism, we might consider a tailored model for 1D decay, which strictly enforces fixed island width. In such an approach, we propose to introduce a separate diffusion field n_{edge} for edge adatoms (cf. Ref. 34) on the ⟨$\bar{1}$10⟩ edges. An equation for the dynamics of this diffusion field accounts for attachment, detachment, edge diffusion, and corner rounding of these edge atoms. Within such a formalism, we can more readily assess, e.g., the conditions under which return of recondensed adatoms to the ⟨001⟩ edge is diffusion limited versus corner rounding limited (cf. Sec. V B). Results from such refined analytic treatments of 1D decay will be presented in a separate publication.

ACKNOWLEDGMENTS

This paper was supported by National Science Foundation Grant No. CHE-1111500. It was performed at Ames Laboratory, which is operated for the US Department of Energy by Iowa State University under Contract No. DE-AC02-07CH11358.

*Present address: Electrochemistry Branch, Power and Energy Division, Sensor and Electron Devices Directorate, US Army Research Laboratory, Adelphi, Maryland 20783, USA.

†Present address: Jannen School of Arts and Sciences, Trine University, One University Avenue, Angola, Indiana 46703, USA.

[1] L. Ratke and P. W. Voorhees, *Growth and Coarsening: Ripening in Materials Processing* (Springer, Berlin, 2001).

[2] K. G. Wang and M. E. Glicksman, *Ostwald Ripening in Materials Processing, in Materials Processing Handbook* (Taylor & Francis, London, 2007).

[3] M. Zinke-Allmang, L. C. Feldman, and M. H. Grabow, Surf. Sci. Rep. **16**, 377 (1992).

[4] K. Morgenstern, Phys. Stat. Sol. B **242**, 773 (2005).

[5] P. A. Thiel, M. Shen, D.-J. Liu, and J. W. Evans, J. Phys. Chem. C **113**, 5047 (2009).

[6] W. Ostwald, *Lehrbuch der Allgemeinen Chemie* (Verlag von W. Engelmann, Leipzig, Germany, 1887), Vol. 2, Part 1.

[7] J. W. Evans, P. A. Thiel, and M. C. Bartelt, Surf. Sci. Rep. **61**, 1 (2006).

[8] K. Morgenstern, E. Lægsgaard, I. Stensgaard, and F. Besenbacher, Phys. Rev. Lett. **83**, 1613 (1999).

[9] K. Morgenstern, E. Lægsgaard, I. Stensgaard, F. Besenbacher, M. Böhringer, W.-D. Schneider, R. Berndt, F. Mauri, A. De Vita, and R. Car, Appl. Phys. A **69**, 559 (1999).

[10]P. A. Thiel, M. Shen, D.-J. Liu, and J. W. Evans, J. Vac. Sci. Technol. A **28**, 1285 (2010).
[11]L. Guillemot and K. Bobrov, Surf. Sci. **601**, 871 (2007).
[12]H. A. Engelhardt and D. Menzel, Surf. Sci. **57**, 591 (1976).
[13]C. Mottet, R. Ferrando, F. Hontininde, and A. C. Levi, Surf. Sci. **417**, 220 (1998).
[14]C. D. Giorgi, P. Aihemaiti, F. B. de Mongeot, C. Boragno, R. Ferrando, and U. Valbusa, Surf. Sci. **487**, 49 (2001).
[15]This result is consistent with application in this system of the standard criterion for irreversible island formation, which is that the rate for in-channel bond breaking is below the rate for aggregation (Ref. 7). However, this criterion is traditionally applied for isotropic systems, where island growth yields additional island stabilization, because most edge adatoms acquire multiple strong bonds, in contrast to the Ag/Ag(110) system.
[16]M. C. Bartelt and J. W. Evans, Europhys. Lett. **21**, 99 (1993).
[17]Y. Li, M. C. Bartelt, J. W. Evans, N. Waelchli, E. Kampshoff, and K. Kern, Phys. Rev. B **56**, 12539 (1997).
[18]Since on average $A \approx \theta A_{CZ}$ for Ag coverage θ, a crude analysis suggests that $\langle L_{sep} \rangle \sim \langle L^{\parallel}_{sep} \rangle \sim \langle L^{\parallel}_{CZ} - L^{\parallel} \rangle \sim [1 - (\theta R/r)^{1/2}] L^{\parallel}_{CZ}$, which is smaller for larger R. See Fig. 3.
[19]L. D. Landau and E. M. Lifshitz, *Course on Theoretical Physics: Statistical Physics* (Permagon, New York, 1959), Vol. 5, p. 482.
[20]Y. Han, J. Y. Zhu, F. Liu, S.-C. Li, J.-F. Jia, Y.-F. Zhang, and Q.-K. Xue, Phys. Rev. Lett. **93**, 106102 (2004).
[21]M. Li, C. Z. Wang, J. W. Evans, M. Hupalo, M. C. Tringides, and K. M. Ho, Phys. Rev. B **79**, 113404 (2009).
[22]A partial chemical potential for $\langle \bar{1}10 \rangle$steps could be obtained similarly as $\mu_{\bar{1}10} = \mu_\infty + 2\Omega\gamma^{\perp}/L^{\parallel}$, with a local equilibrium adatom density $n_{\bar{1}10} = n_\infty \exp(2\beta\Omega\gamma^{\perp}/L^{\parallel})$, but this is not relevant for purely 1D decay.
[23]Y. Yao, Ph. Ebert, M. Li, Z. Zhang, and E. G. Wang, Phys. Rev. B **66**, 041407 (2002). Note the typographic error in the expressions for equilibrium adatom densities at island edges (cf. Sec. IVB).
[24]For 2D island decay in our anisotropic system at higher T above 220 K, this result is naturally replaced by $E_{OR} = (E^{\parallel}_d + E^{\perp}_d)/2 + E_{form}$.
[25]R. Ferrando, F. Hontinfinde, and A. C. Levi, Phys. Rev. B **56**, R4406 (1997).
[26]Simulated island morphologies just after deposition appear to match STM images. However, the latter are obtained perhaps 10 min after deposition. We find that postdeposition evolution of island morphologies for ∼10 min gives poorer agreement with STM.
[27]T. Duguet, Y. Han, C. Yuen, D. Jing, B. Ünal, J. W. Evans, and P. A. Thiel, Proc. Nat. Acad. Sci. **108**, 989 (2011).
[28]Y. Han, B. Ünal, D. Jing, P. A. Thiel, and J. W. Evans, J. Chem. Phys. **135**, 084706 (2011).
[29]Y. Han, D. Jing, B. Ünal, P. A. Thiel, and J. W. Evans, Phys. Rev. B **84**, 113414 (2011).
[30]F. Hontinfinde, R. Ferrando, and A. C. Levi, Surf. Sci. **366**, 306 (1996).
[31]See Supplemental Material at http://link.aps.org/supplemental/10.1103/PhysRevB.87.155420 for atom-tracking KMC simulation movies of Ag island decay on Ag(110) corresponding to the green curves in Fig. 11(a) (Fig. 11a.wmv) and Fig. 11(b) (Fig. 11b.wmv) and the red curve in Fig. 11(c) (Fig. 11c.wmv). Readers can view the movie files using Windows Media Player, RealPlayer, etc.
[32]H.-C. Jeong and E. D. Williams, Surf. Sci. Rep. **34**, 171 (1999).
[33]D. M. Ackerman and J. W. Evans, Multiscale Model. Simul. **9**, 59 (2011).
[34]R. E. Caflisch, E. Weinan, M. F. Gyure, B. Merriman, and C. Ratsch, Phys. Rev. E **59**, 6879 (1999).